Available online at www.sciencedirect.com

ScienceDirect

Materials Today: Proceedings XX (2017) XXX–XXX

materialstoday: PROCEEDINGS

www.materialstoday.com/proceedings

ANM2017

Synthesis of ZnO mesoporous powders and their application in dye photodegradation

Hanna Maltanava[a]*, Sergey Poznyak[a], Evgeni Ovodok[a], Maria Ivanovskaya[a], Frederico Maia[b], Alexander Kudlash[c], Nico Scharnagl[d], João Tedim[e]

[a]*Research Institute for Physical Chemical Problems, Belarusian State University, Leningradskaya str. 14, 220030 Minsk, Belarus*
[b]*Smallmatek, Small Materials and Technologies, Portugal*
[c]*Faculty of Chemistry, Belarusian State University, Nezavisimosti ave. 4, 220030 Minsk, Belarus*
[c]*Helmholtz-Zentrum Geesthacht, Centre for Materials and Coastal Research GmbH, Max-Planck-Straße 1, 21502 Geesthacht, Germany*
[d]*Department of Materials and Ceramics Engineering, CICECO-Aveiro Institute of Materials, The University of Aveiro, Campus Universitário de Santiago, 3810-193 Aveiro, Portugal*

Abstract

Mesoporous ZnO materials have been synthesized through chemical deposition of different precursors from aqueous or water-ethanol solutions followed by their thermal decomposition at 400°C in air. The microstructure and morphology of the precursors and obtained ZnO powders were characterized by X-ray powder diffraction (XRD), scanning electron microscopy (SEM), transmission electron microscope (TEM) and nitrogen adsorption-desorption (BET) methods. The structure of the precursor and physico-chemical properties of final zinc oxide powders were shown to be considerably influenced by the presence of Cl^- ions and ethanol in solution. In water-ethanol solutions, $Zn_5(OH)_8Cl_2{\cdot}H_2O$ or $Zn_5(OH)_8(NO_3)_2{\cdot}(H_2O)_2$ precursors are formed, while ZnO particles are directly deposited from aqueous solution. The photocatalytic activity of the synthesized ZnO materials was evaluated by the decolorization of Rhodamine B (RhB) upon UV irradiation. The ZnO powders have demonstrated high photocatalytic efficiency, enabling decomposition of 81.4–97.4 % RhB within 3 hours. The increased photocatalytic efficiency of ZnO prepared by annealing of $Zn_5(OH)_8Cl_2{\cdot}H_2O$ precursor or deposited directly from aqueous chloride-containing solutions can be originated from the presence of Cl-containing compounds remaining after thermal treatment of simonkolleite as well as from introduction of Cl-dopant in ZnO.

Selection and/or Peer-review under responsibility of ANM2017.

Keywords: Zinc oxide; Simonkolleite; Chemical precipitation; Photocatalysis

* Corresponding author. Tel.: +3-751-720-953-02.
E-mail address: annamaltanova@gmail.com

1. Introduction

Among metal oxide semiconductors, zinc oxide is extensively studied material with large-scale potential applications owing to its high thermo-mechanical stability, good piezoelectric, optoelectronic, catalytic and ferromagnetic properties [1, 2]. Beside the attractive physico-chemical characteristics, ZnO is also nontoxic, cheap and chemically stable material [3, 4]. The properties of synthesized ZnO materials correlate with shape, size, defect structure and crystallinity of their particles [5−9]. Therefore, the structural or morphologic modifications of ZnO are crucial issues in terms of research as well as further application of synthesized materials.

Although to a lesser extent as compared with well-known TiO_2, ZnO nanostructured materials have also received considerable interest for photocatalytic applications [5, 6, 10−15]. ZnO with different structure and morphology was synthesized and applied to eliminate harmful dyes by photocatalytic reaction under UV illumination. Rahman et al. demonstrated effective degradation of Rhodamine B (~ 95% within 70 min) in the presence of highly uniform spherical ZnO nanoparticles. Sun et al. [12] and Kuo et al. [13] exhibited the photocatalytic degradation of methyl orange (~94%) and Rhodamine B dyes in 5 h under UV irradiation over the surface of ZnO nanobelts and ZnO nanowires. Alvi et al. investigated the photocatalytic activity of ZnO rods toward RhB photodegradation and showed a rapid degradation rate (~97% RhB decomposed in 120 min) [14]. For photocatalytic applications, ZnO is usually prepared with a porous structure, providing a large surface area and a high crystallinity for enhancing the system performance [16−18]. However, the size as well as the shape of the photocatalyst particles also influence the efficiency of photodegradation of hazardous organic compounds [5, 6, 19]. Wolski et al. have recently shown the correlation between photocatalytic activity and morphology, structure and surface peculiarities of ZnO photocatalysts [6].

Various methods have been explored to prepare ZnO porous powders and films such as vapour transport process, pulse laser ablation, magnetron sputtering, vacuum evaporation, spray pyrolysis, thermal decomposition, hydrothermal synthesis, sol-gel processing, direct precipitation and etc. [2]. Among these methods, commonly used physical techniques like magnetron sputtering or vapour deposition have some disadvantages such as multiple steps, large energy consumption, high temperature processing, sophisticated and expensive equipment [20]. At the same time, wet chemical methods, including precipitation from inorganic or organic solutions, hydrothermal process and sol-gel, are simple and low cost. In particularly, the precipitation approach has been utilized to fabricate various structures of ZnO [2, 9, 21−23]. Different factors, such as reaction temperature, time, concentration of reagents, pH, capping molecules, were reported to affect the microstructure of the ZnO particles prepared by precipitation process [2, 24−26]. Also, solvents can strongly affect ZnO crystal growth and morphology of the final products [27−29].

Herein, we synthesized ZnO mesoporous powders by the precipitation method. The attention was given to the role of reaction medium and precursors in the formation of final products. In addition, we estimated photocatalytic activity of the prepared ZnO powders towards photodegradation of Rhodamine B under UV irradiation.

2. Experimental

The synthesis of mesoporous ZnO powders was based on preparation and further thermal decomposition of zinc hydroxide chloride precursor ($Zn_5(OH)_8Cl_2{\cdot}H_2O$) or other precursors.

In a typical procedure to fabricate $Zn_5(OH)_8Cl_2{\cdot}H_2O$ precursor, 29.7 g of $Zn(NO_3)_2{\cdot}6H_2O$, 7.45 g of KCl and 10 g of polyvinylpyrrolidone (PVP) were dissolved in 1 L of water-ethanol mixture (50:50 by vol.). The mixed solution was transferred into a three necked round bottom flask and gradually heated on glycerol bath to 70ºC with stirring. Aqueous ammonia solution (8.25 %) was added dropwise into the reaction solution with stirring until pH value of 7.0. The resultant solution was kept with stirring at 70ºC for 6h. After cooling down to room temperature, the obtained precipitate was filtered, rinsed with distilled water 2 times and then dried at 50^{o}C in air. In order to define the role of different components ($Zn(NO_3)_2$, KCl, PVP and ethanol) of the solution in preparation of the precursor for ZnO synthesis, a set of experiments with different composition of the reaction solution was carried out. . Composition of the solutions in these experiments is presented in Table 1. Molar ratio of initial components and reaction conditions were identical in all series. The resulting powders were annealed at 400^{o}C for 1 h in the stream of air.

Table 1. Series of ZnO mesoporous powders and composition of the reaction solution for their synthesis.

Samples	Composition of the reaction solution
Z1	$Zn(NO_3)_2$, KCl, PVP, ethanol-water
Z2	$Zn(NO_3)_2$, KCl, ethanol-water
Z3	$Zn(NO_3)_2$, ethanol-water
Z4	$ZnCl_2$, ethanol-water
Z5	$Zn(NO_3)_2$, KCl, PVP, water

The morphology of the samples was studied using a Hitachi-4100 scanning electron microscope (SEM) and a LEO-640 transmission electron microscope (TEM).

The crystal structure was examined by X-ray diffraction on a PANalytical X'Pert PRO MRD (Multi-Purpose Research Diffractometer, Holland) with modular construction using CuKα-radiation. Recording speed was 0.4 °/min.

The surface area and porosity of the samples were measured on a Micromeritics ASAP 2020 system using nitrogen at 77 K.

Energy dispersive X-ray fluorescence measurements were performed using an Epsilon 1 EDXRF spectrometer, equipped with a 50 kV silver anode X-ray tube, 6 filters and high-resolution silicon drift detector. Automatic data processing was performed using the Epsilon 3 software

The photocatalytic activity of the ZnO powders was evaluated by the decolorization of RhB (a typical organic azo-dye pollutant in the textile industry) upon UV irradiation. In a typical photocatalytic reaction, 100 mg of ZnO catalyst was dispersed in 100 mL of 0.02 mM RhB aqueous solution in a quartz cylindrical reactor. The reaction mixture was then stirred in the dark for 1 h in order to establish adsorption-desorption equilibrium between the catalyst surface and the dye. The suspension was irradiated with a mercury lamp (Narva UVK-125-2) with emission centred at 365 nm for 3 h. The suspension was slightly stirred using a magnetic stirrer during the irradiation. The absorbance of the RhB solution was measured after 1h of stirring in the dark and after 10−60, 90, 120, 150, 180 min of irradiation. After the reaction mixture was irradiated for a given time, a 1 ml aliquot was withdrawn and the catalyst was separated from solution by centrifugation at 10000 rpm. The absorption spectrum of the clear supernatant was recorded using UV–Vis spectroscopy, and the RhB conversion was calculated using the following equation:

$$RhB\ conversion = \frac{C_0 - C}{C_0} \times 100\% = \frac{A_0 - A}{A_0} \times 100\% \quad (1)$$

where A_0 is the absorbance of RhB solution measured after 1 h of stirring in the dark, A is the absorbance of the RhB solution after a given time of irradiation with UV light. The absorbance was measured at 552 nm.

3. Result and discussions

The XRD data indicate that a pure phase of $Zn_5(OH)_8Cl_2{\cdot}H_2O$ is formed during the hydrolytic reaction of $Zn(NO_3)_2$ in KCl-containing water-ethanol solution (Fig. 1). Only simonkolleite ($Zn_5(OH)_8Cl_2{\cdot}H_2O$) is also deposited in $ZnCl_2$ water-ethanol solution. After annealing at 400 °C in air, the $Zn_5(OH)_8Cl_2{\cdot}H_2O$ precursor transforms into wurtzite ZnO (Fig. 1). However, the admixture of $Zn_5(OH)_8Cl_2{\cdot}H_2O$ and Zn(OH)Cl phases is also found in the annealed samples. The role of ethanol was studied by replacement of water-ethanol mixture with aqueous solutions. In this case, the hydrolytic reaction of $Zn(NO_3)_2$ in KCl-containing solution led to the formation of precipitate consisting of pure ZnO (Fig. 2). It is worth mentioning that hydrolytic reaction of $Zn(NO_3)_2$ in chloride-free water-ethanol solution gives the mixture of $Zn_5(OH)_8(NO_3)_2{\cdot}(H_2O)_2$ and ZnO. After annealing zinc hydroxide nitrate decomposes forming ZnO (Fig. 2). The addition of PVP into the solution does not influence the composition of precipitates, but reduces the crystal size of the final ZnO product as will be shown below. All as-synthesized precursors and resulting products obtained after annealing of the precursors are summarized in Table 2.

The average size of ZnO wurtzite crystallites was estimated by the width of the (101) peak using Debye–Scherrer equation ($D = 0.9\lambda/k\cos\theta$, where k is the full width at half-maximum (FWHM) of the peak, θ is the angle of

diffraction, and λ is the wavelength of the X-ray radiation) and the obtained data are collected in Table 2. ZnO powders (Z1, Z2, Z4) prepared through thermal decomposition of $Zn_5(OH)_8Cl_2{\cdot}H_2O$ precursor consist of smaller particles than ZnO (Z3) obtained by annealing of $Zn_5(OH)_8(NO_3)_2{\cdot}(H_2O)_2$ precursor. Also, the relative degree of crystallinity of different ZnO powders was determined by comparison of the intensity of the peak assigned to the (101) plane of the synthesized powders with the most intensive peak observed for ZnO (Z3) prepared from $Zn_5(OH)_8(NO_3)_2{\cdot}(H_2O)_2$ precursor, which was taken for 100%. The relative degree of crystallinity for Z1, Z2, Z4 and Z5 samples after annealing was 71%, 84%, 92% and 65%, respectively.

Table 2. Precursors, final products after precursor's annealing and characteristics of the final products for different experimental series

Samples	Precursors	Final products	Color of final products	ZnO crystal size (nm)	BET surface area (m^2/g)	Pore diameter (nm)	RhB conversion (%)
Z1	$Zn_5(OH)_8Cl_2{\cdot}H_2O$	ZnO, $Zn_5(OH)_8Cl_2{\cdot}H_2O$, Zn(OH)Cl	gray	28.1	16.7	11.2	94.9
Z2	$Zn_5(OH)_8Cl_2{\cdot}H_2O$	ZnO, $Zn_5(OH)_8Cl_2{\cdot}H_2O$, Zn(OH)Cl	yellow-light	33.4	14	8.2	97.1
Z3	$Zn_5(OH)_8(NO_3)_2{\cdot}(H_2O)_2$ + several percent of ZnO	ZnO	pink-light	66.1	9.8	6.5	81.4
Z4	$Zn_5(OH)_8Cl_2{\cdot}H_2O$	ZnO, $Zn_5(OH)_8Cl_2{\cdot}H_2O$, Zn(OH)Cl	yellow-light	31.3	13.6	8.8	90.8
Z5	ZnO	ZnO	gray-light	35.0	7.2	7.3	97.4

Considering the above mentioned results, we can conclude that the structure of the as-prepared precipitate strongly depends on the presence of ethanol and Cl^- anions in the solution. The influence of ethanol on the precursor formation may be explained by the participation of ethanol molecules in hydrolytic reactions of Zn^{2+} in the solution. Generally, ammonia reacts with water to form ammonia hydroxide, generating OH^- ions. Hydroxyl ions interact with Zn^{2+}, producing hydroxide species: $Zn(OH)^+(aq)$, $Zn(OH)_2(aq)$, $Zn(OH)_2(s)$, $Zn(OH)_3^-(aq)$ and $Zn(OH)_4^{2-}(aq)$. The nuclei of ZnO start growing by dehydration of these hydroxide species. It seems unlikely that Zn^{2+} ions can form any complexes with ethanol molecules, but C_2H_5OH can affect the hydrolytic reactions involving Zn^{2+} ions. In particular, ethanol can facilitate the precipitation of one product and decrease the solubility of other one [30]. The structure of the precursor also depends on the presence of chloride ions in the solution. In the absence of KCl, zinc hydroxide nitrate hydrate and zinc oxide were obtained (Table 2). But, the presence of Cl^- in the solution promotes simonkolleite formation.

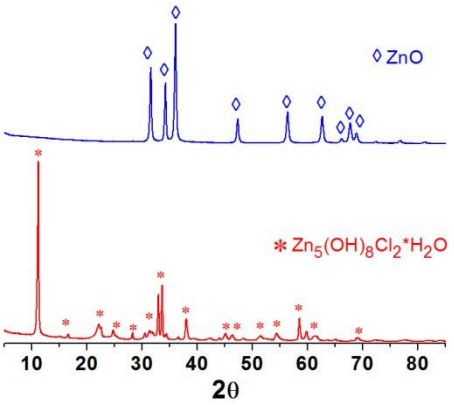

Fig. 1. X-ray diffractograms of zinc hydroxide chloride precursor and zinc oxide powder obtained after precursor calcination at 400°C.

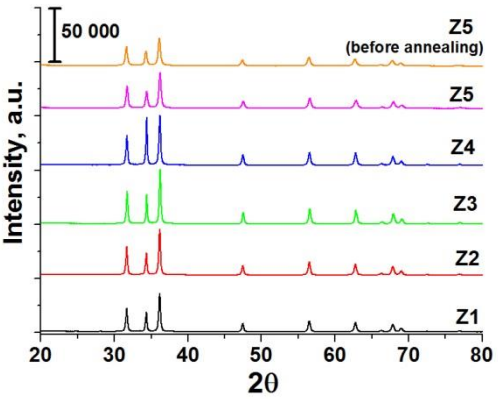

Fig. 2. X-ray diffractograms of zinc oxide powders

To study the effect of synthetic conditions on the morphology, SEM and TEM images were taken for the different zinc oxide samples and their precursors, which are presented in Figs. 3 – 5. SEM images show that zinc hydroxide chloride precursor is comprised of microplates with a lateral size of 0.5 – 1.5 μm and a thickness of 100 – 200 nm (Fig. 3a). During annealing of the samples the microplate shape is preserved, but each sheet consists of a great number of finest particles having a size of 20 – 40 nm (Fig. 3b, inset). However, thermal treatment of zinc hydroxide chloride precursor synthesized without PVP leads to some consolidation of primary microplates (Fig. 3c, d). The zinc oxide deposit obtained from aqueous solution exhibits significantly different morphology and consists of well-faceted hexagonal particles with a diameter of 29÷146 nm and a length of 29÷85 nm (Fig. 4). As it was reported previously [31, 32], PVP can control the shape and the size of the resultant particles, suppressing the growth of ZnO nuclei along the polar [0001] direction.

Typical TEM image of as-prepared products grown in chloride-free water-ethanol solution is shown in Figure 5. It reveals that some amount of well-defined rectangle sheets and hexagonal columns are formed simultaneously. Sheet-like morphology is characteristic of $Zn_5(OH)_8(NO_3)_2{\cdot}(H_2O)_2$ crystals, which have the laminar structure similar to layered double hydroxide salts. Hexagonal columns are ZnO crystals formed through $Zn(OH)_2$ or $Zn(OH)_4^{2-}$ decomposition during the hydrolytic reaction.

Fine-crystalline structure of the prepared ZnO powders imparts them a high specific surface area. The isotherms of nitrogen adsorption-desorption of all materials belong to type IV with a distinct hysteresis loop, which is characteristic of mesoporous materials. The BET surface area (S_{BET}) and the average pore size of the annealed samples are presented in Table 2. The S_{BET} of the produced ZnO powders was 7.2−16.7 m^2/g that is typical for ZnO formed by direct wet-chemistry precipitation techniques (~10−33 m^2/g) [33] and is higher in comparison with common industrial French process (~3−5 m^2/g) [34], but lower than that reported for ZnO obtained by decomposition of zinc hydroxide carbonate (47−65 m^2/g) [33].

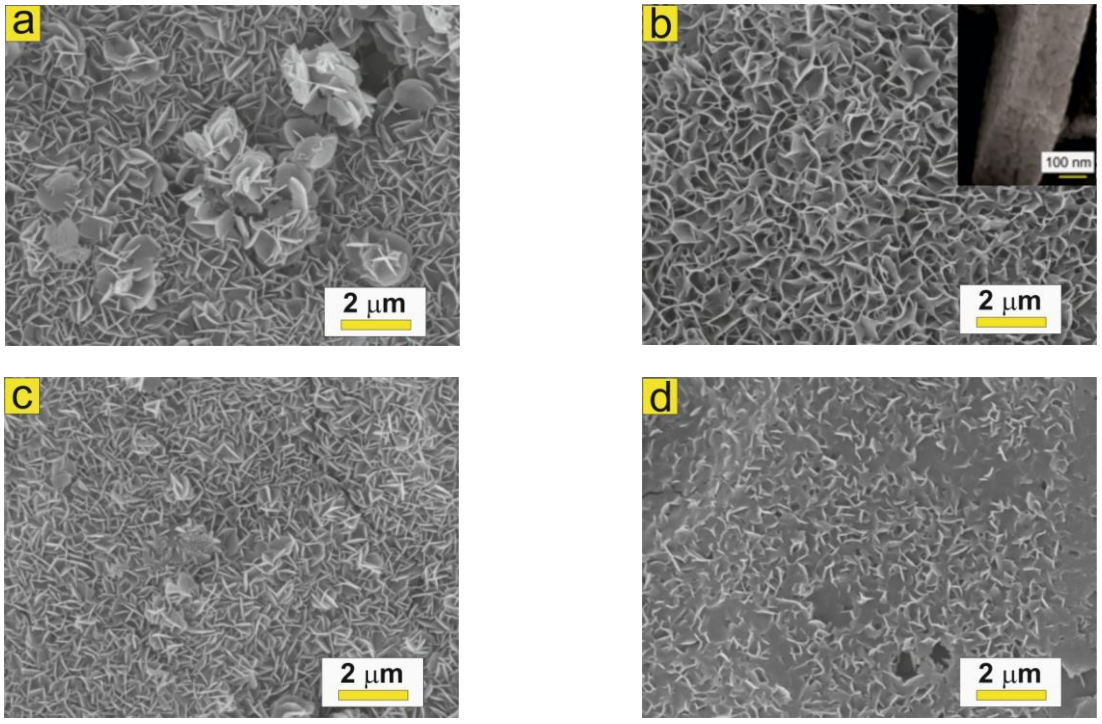

Fig.3. SEM images of simonkolleite precursors (*a*, *c*) deposited from water-ethanol solution containing $Zn(NO_3)_2$ and KCl with (*a*) and without PVP (*c*) and ZnO powders after annealing (*b*, *d*)

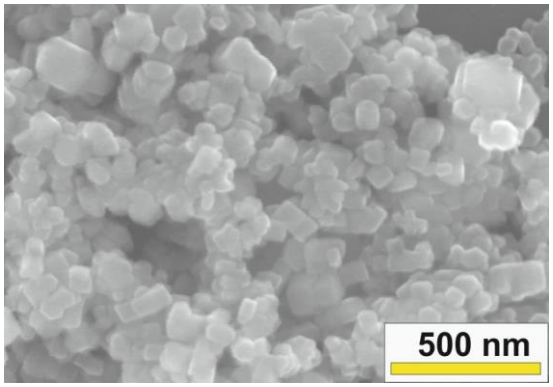

Fig. 4 SEM image of ZnO powder produced from aqueous solution containing $Zn(NO_3)_2$, KCl and PVP.

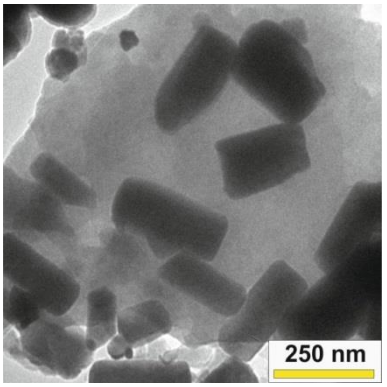

Fig.5 TEM image of precursor particles prepared from water-ethanol solution containing $Zn(NO_3)_2$.

It is clearly demonstrated that varying the synthetic conditions significantly affects the specific surface area and pore size distribution of the resultant ZnO powders. The highest S_{BET} (16.7 m^2/g) was measured for the sample Z1, slightly lower value (14 m^2/g) was observed for the sample Z2. Both these samples were obtained by thermal decomposition of simonkolleite precursor deposited from water-ethanol solution containing $Zn(NO_3)_2$ and KCl as initial compounds. The presence of PVP in the reaction solution promotes an increase of the surface area of obtained ZnO (sample Z1). The ZnO powders formed by thermal decomposition of zinc hydroxide nitrate have *ca.* two times lower S_{BET} that also correlates with the crystal size calculated using Debye–Scherrer equation. The zinc oxide

obtained directly from aqueous solution exhibits the lowest S_{BET} values (7.2 m^2/g) that can prove the essential role of intermediate simonkolleite precursor in the formation of ZnO powders with developed structure.

Figure 6 represents photocatalytic efficiency of the synthesized ZnO powders toward degradation of RhB under UV illumination. After exposure for 3 h, 81.4–97.4 % of RhB was decomposed, indicating the excellent photocatalytic activity of all ZnO powders. Characteristically, the samples prepared from chloride-containing solutions demonstrate rather similar photocatalytic efficiency. At the same time, Z3 powder obtained by thermal decomposition of $Zn_5(OH)_8(NO_3)_2$ precursor is less active as compared with other powders. The enhanced photocatalytic activity of the ZnO powders prepared by annealing of $Zn_5(OH)_8Cl_2{\cdot}H_2O$ precursor can be related to the presence of Cl-containing compounds remaining after thermal decomposition of simonkolleite [35] as well as chlorine doping of ZnO [36]. The chlorine content in the ZnO powders was determined by energy dispersive X-ray fluorescence technique. The ZnO powders synthesized via decomposition of simonkolleite were found to contain approximately 2 wt. % of chlorine. Furthermore, the ZnO sample directly obtained from aqueous solution (Z5) also holds *ca.* 0.87 wt.% of chlorine.

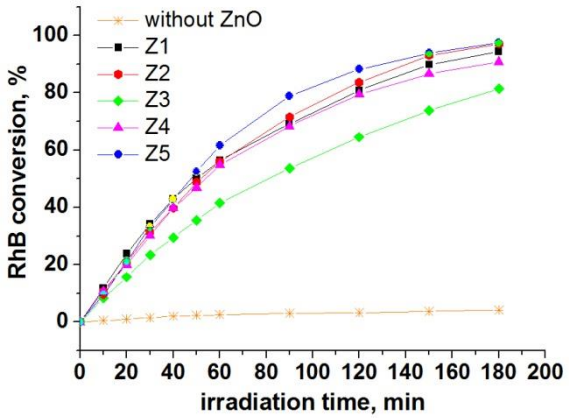

Fig. 6. Photodegradation of RhB over ZnO powders

Upon UV irradiation, the generation of electron-hole pairs occurs between conduction (CB) and valence band (VB) of ZnO particles. Photogenerated electrons in the CB move toward the oxide surface to produce O_2^- anions followed by formation of protonated $HOO^{\cdot}$ radicals. At the same time, holes in the VB migrate to other side of the ZnO particle and react either with H_2O or OH^- forming very reactive species such as $OH^{\cdot}$. Generated active oxygen species (O_2^-, $HOO^{\cdot}$, $OH^{\cdot}$) are responsible for transformation of RhB into less harmful organics or mineralized products. The Cl doping of ZnO was reported to create a higher density of surface defects in the oxide [36]. The surface defects of ZnO can act as efficient hole trapping centers and, hence, reduce the recombination probability of photogenerated electron-hole pairs. These factors can provide the increased photocatalytic performance of chlorine-doped ZnO powders.

4. Conclusion

The synthesis of mesoporous ZnO powders based on the chemical precipitation of different precursors, such as $Zn_5(OH)_8Cl_2{\cdot}H_2O$ or $Zn_5(OH)_8(NO_3)_2{\cdot}(H_2O)_2$, and their further thermal decomposition has been described. Structural and morphological peculiarities of the precursors and final ZnO powders were found to depend strongly on initial components of solution ($Zn(NO_3)_2$ or $ZnCl_2$, KCl, PVP and ethanol). The simonkolleite precursor with a plate-like morphology was obtained via precipitation from chloride-containing water-ethanol solutions. The precipitation from the aqueous solution containing $Zn(NO_3)_2$ and KCl resulted in the formation of pure ZnO with well-faceted hexagonal particles. At the same time, chloride-free water-ethanol solution gave the mixture of $Zn_5(OH)_8(NO_3)_2{\cdot}(H_2O)_2$ and ZnO. The specific surface area of the resulting ZnO powders was larger for the samples

obtained from simonkolleite precursor. The photocatalytic activity of the ZnO powders was evaluated toward degradation of RhB under UV illumination. The samples obtained from chloride-containing water-ethanol or aqueous solutions demonstrated rather similar photocatalytic activity. At the same time, ZnO obtained by thermal decomposition of $Zn_5(OH)_8(NO_3)_2{\cdot}(H_2O)_2$ precursor was less active as compared with other powders. The enhancement of photocatalytic efficiency of the ZnO powders prepared from chloride-containing solutions can be related to the favorable effect of $Zn_5(OH)_8Cl_2{\cdot}H_2O$/ZnO heterostructures or chlorine doping of ZnO on the separation of photogenerated charge carriers in ZnO crystals.

Acknowledgements

We acknowledge funding from SMARCOAT project. This project has received funding from the European Union's Horizon 2020 research and innovation programme under the Marie Skłodowska-Curie grant agreement No 645662. This work was also developed in the scope of the project CICECO – Aveiro Institute of Materials, POCI-01-0145-FEDER-007679 (Ref. FCT UID/CTM/50011/2013), financed by national funds through the FCT/MEC and when applicable co-financed by FEDER under the PT2020 Partnership Agreement. JT thanks FCT for the research grant IF/00347/2013.

References

[1] Ü. Özgür, Ya. I. Alivov, C. Liu, A. Teke, M. A. Reshchikov, S. Doğan, V. Avrutin, S.-J. Cho, H. Morkoç, J. Appl. Phys. 98 (2005) 041301-1−041301-103.
[2] A. Kołodziejczak-Radzimska, T. Jesionowski, Materials 7 *(*2014) 2833−2881.
[3] H. Morkoç, Ü. Özgür, Zinc Oxide: Fundamentals, Materials and Device Technology, first ed., WILEY-VCH, Berlin, 2009.
[4] A. Sirelkhatim, S. Mahmud, A. Seeni, N.H.M. Kaus, L. C. Ann, S. K. M. Bakhori, H. Hasan, D. Mohamad, Nano-Micro Letters *7*(3) (2015) 219-242.
[5] A. Mclaren, T. Valdes-Solis, G. Li, S. C. Tsang, J. Am. Chem. Soc. 131 (35) (2009), 12540–12541.
[6] L. Wolski, J.E. Whitten, I. Sobczak, M. Ziolek, Mater. Res. Bull. 85 (2017) 35−46.
[7] V. Ischenko, S. Polarz, D. Grote, V. Stavarache, K. Fink, Adv. Funct.Mater. 15 (2005) 1945−1954.
[8] Y. Zheng, C. Chen, Y. Zhan, X. Lin, Q. Zheng, K. Wei, J. Zhu, Y. Zhu, Inorg. Chem. 46 (16) (2007) 6675–6682.
[9] S.Musić, Đ.Dragčević, S.Popović, M.Ivanda, Mater. Lett. 59 (2005) 2388–2393.
[10] Q.I. Rahman, M. Ahmad, S.K. Misra, M. Lohani, Mater. Lett. 91 (2013) 170–174.
[11] A. C. Dhayagude, S. V. Nikam, S. Kapoor, S. S. Joshi, J. Mol. Liq. 232 (2017) 290–303.
[12] T. Sun, J. Qiu, C. Liang, J. Phys. Chem. C 112 (3) (2008) 715–721.
[13] T.-J. Kuo, C.-N. Lin, C.-L. Kuo, M. H. Huang, Chem. Mater. 19 (2007) 5143−5147.
[14] M.A. Alvi, A.A. Al-Ghamdi, M. ShaheerAkhtar, Mater. Lett. 204 (2017) 12−15.
[15] J.Wang, J. Yang, X. Li, B. Feng, B.Wei, D.Wang, H. Zhai, H. Song, Powder Technol. 286 (2015) 269–275.
[16] D. An, Y. Li, X. Lian, Y. Zou, G. Deng, Colloids and Surfaces A: Physicochem. Eng. Aspects 447 (2014) 81–87.
[17] E.S. Elmolla, M. Chaudhuri, J. Hazardous Mater. 173 (2010) 445–449.
[18] F. Xu, P. Zhang, A. Navrotsky, Z.Y. Yuan, T.Z. Ren, M. Halasa, B.L. Su, Chem. Mater. 19 (2007) 5680–5686.
[19] N. Morales-Flores, U. Pal, R. Galeazzia, A. Sandovalb, RSC Adv. 4 (2014) 41099-41110.
[20] D. Raoufi, Renew. Energy 50 (2013) 932−937.
[21] S. Sepulveda-Guzman, B. Reeja-Jayan, E. de la Rosa, A. Torres-Castro, Mater. Chem. Phys. 115 (2009) 172−178.
[22] M. Iwasaki, Y. Inubushi, S. Ito, J. Mater. Sci. Lett. 16 (1997) 1503−1505.
[23] A.S. Lanje, S.J. Sharma, R.S. Ningthoujam, J.S. Ahn, R.B. Pode, Adv. Powder Technol. 24 (2013**)** 331–335.
[24] A. Kołodziejczak-Radzimska, T. Jesionowski, A. Krysztafkiewicz, Physicochem. Probl. Miner. Process. 44 (2010**)** 93–102.
[25] N. Samaele, P. Amornpitoksuk, S. Suwanboon, Powder Technol. 203 (2010) 243−247.
[26] Y. Wang, C. Ma, X. Sun, H. Li, Inorg. Chem. Commun. 5 *(*2002) 751–755.
[27] P. Uthirakumar, B. Karunagaran, S. Nagarajan, E.-K. Suh, C.-H. Hong, J. Cryst. Growth 304 (2007) 150–157.
[28] E. Hosono, S. Fujihara, T. Kimura, H. Imai, J. Sol-Gel Sci. Technol. 29(2) (2004) 71–79.
[29] P.B. Khoza, M.J. Moloto, L.M. Sikhwivhilu, J. Nanotechnol. (2012) 1–6.
[30] C.-H. Ho, J. W. Van Zee, Ind. Eng. Chem. Res. 39 (3) (2000) 752–758.
[31] B. Panigrahy, M. Aslam, D. S. Misra, D. Bahadur, Cryst. Eng. Comm. 11 (2009) 1920-1925.
[32] M. Eskandari, V. Ahmadi, SH. Ahmadi, Physica B 404 (2009) 1924–1928.
[33] A. Moezzi, M. Cortie, A. McDonagh, Dalton Trans., 40 (2011) 4871–4878.
[34] A. Moezzi, A. M. McDonagh and M. B. Cortie, Chem. Eng. J., 185–186 (2012) 1–22.
[35] H. Chen, L. Zhu, H. Liu, W. Li, Electrochim. Acta 105 (2013) 289– 298.
[36] D. Shao, J. Gao, G. Xin, Y. Wang, L. Li, J. Shi, J. Lian, N. Koratkar, S. Sawyer, Small 11(36) (2015) 4785–4792.